Section 8

Development of and advances in ocean, sea-ice, and wave modelling and data assimilation.

Modular Data Assimilation System for Significant Wave Height: The Example of Local Ensemble Transform Kalman Filter for the National Weather Service

Stylianos Flampouris[1] and Stephen G. Penny[2]

[1] IM Systems Group, College Park, MD, USA; [2]University of Maryland, College Park, MD, USA

Email: stylianos.flampouris@noaa.gov

Introduction

The National Centers for Environmental Prediction (NCEP) of the National Oceanic and Atmospheric Administration (NOAA) provides the operational wave forecast for the U.S. National Weather Service (NWS). As part of ongoing efforts to improve forecasting, the NCEP's Environmental Modeling Center (EMC) is developing an ensemble-based data assimilation system, based on the Local Ensemble Transform Kalman Filter (LETKF) [1], the existing operational Global Wave Ensemble System (GWES) [2], and the operationally available satellite and in-situ observations.

Methodology

The data assimilation system is modular and driven externally by a bash script. A flowchart of the system, including its modules and advantages is shown in Figure 1. The LETKF is a computationally efficient implementation of the varied Ensemble Kalman Filter methods. It uses an ensemble of numerical forecast model runs to estimate the background error covariance and assimilates observations when they occur rather than aggregating them at a fixed analysis. In order to apply LETKF to the wave field, the LETKF system developed for ocean models [3] was adapted to meet the wave field data assimilation requirements; significant wave height (SWH) is assimilated in this case. The forward operator for the SWH is an independent module which handles in-situ and altimeter observations of SWH from four satellites (Jason-2, Jason-3, CryoSat-2 and Saral/Altika, approximately 240k observations per day) and includes a multi-step quality control procedure.
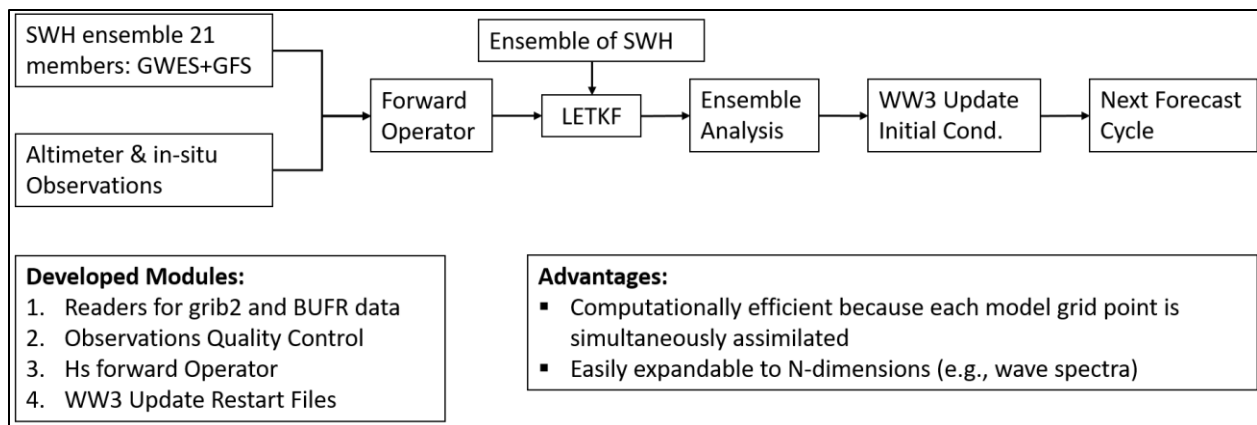
Figure 1. Upper: Flowchart of the modular LETKF DA system for SWH in the framework of the NWS operational guidance. Lower Left: List of the developed modules transferable any wave DA system. Lower Right: List of major advantages of the system.

The GWES is based on WAVEWATCHIII® [4] and it consists of a 20-member ensemble forced with NCEP-GEFS bias corrected wind data, and one control run with NCEP's deterministic GFS model. Each member runs on a spherical grid with 0.5 degree resolution in longitude and latitude, and

uses the ST4 wave physics. In this report, results from a similar system for the Gulf of Mexico with spatial resolution 0.25 degrees are presented.

Results

Results from the LETKF-Wave prototype for three consecutive forecast cycles from the April 6, 2017 are shown in Figure 2. The bias of the analysis has been reduced significantly, at least 100 percent in most of the cases. The preliminary results show that using SWH analysis fields as initial conditions for the next prediction cycle is significant for 12h.
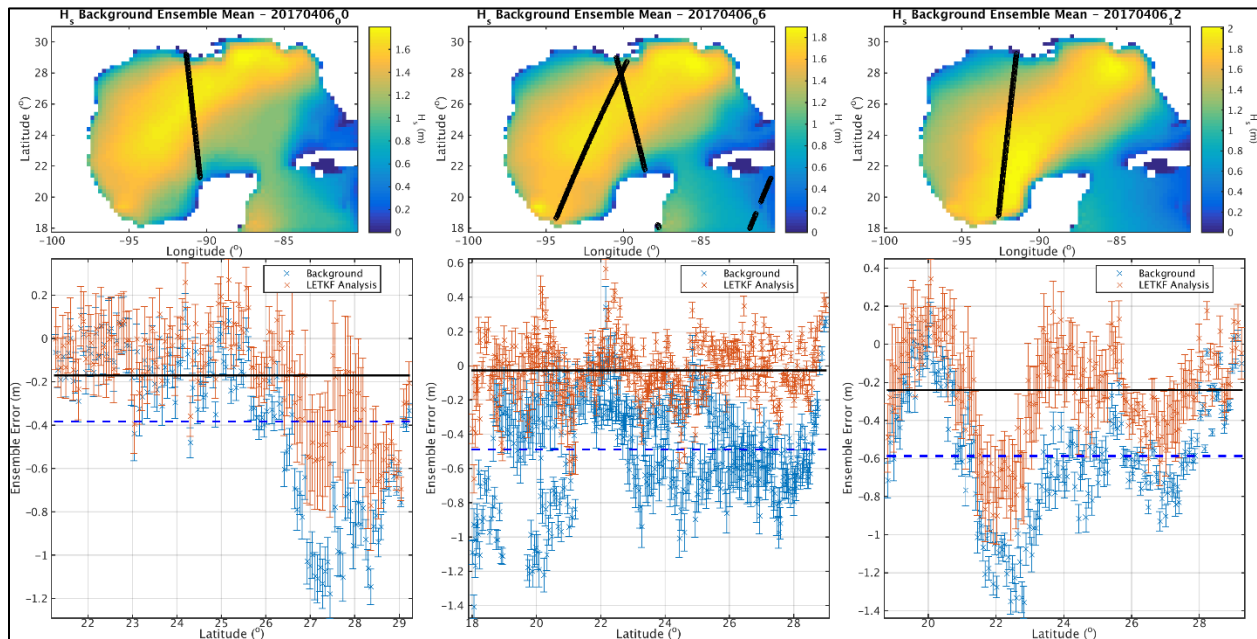
Figure 2. Upper panel: The predicted field of SWH, the black cycles show the locations for the satellites observations. Lower panel: The mean difference of the observed SWH from the background (blue) and the analysis (orange) at the observation locations as function of latitude; the error bars show the spreading of the ensemble. The blue dashed line and the black solid line are the mean bias of background and analysis accordingly.

Summary

The preliminary results from the wave data assimilation suite show great potential for improved NWS wave forecasts. This modular approach is compatible with variational and ensemble-based approaches and is easily expandable. Currently, the LETKF for SWH is under extensive validation and verification at a global scale.

References

[1] Hunt, B. R., Kostelich, E. J., and Szunyogh, I.: Efficient Data Assimilation for Spatiotemporal Chaos: A Local Ensemble Transform Kalman Filter, Phys. D, 230, 112–126, 2007.

[2] Alves, J.G., P. Wittmann, M. Sestak, J. Schauer, S. Stripling, N.B. Bernier, J. McLean, Y. Chao, A. Chawla, H. Tolman, G. Nelson, and S. Klotz, 2013: The NCEP–FNMOC Combined Wave Ensemble Product: Expanding Benefits of Interagency Probabilistic Forecasts to the Oceanic Environment. Bull. Amer. Meteor. Soc., 94, 1893–1905.

[3] Penny, S. G., Kalnay, E., Carton, J. A., Hunt, B. R., Ide, K., Miyoshi, T., and Chepurin, G. A.: The local ensemble transform Kalman filter and the running-in-place algorithm applied to a global ocean general circulation model, Nonlin. Processes Geophys., 20, 1031-1046.

[4] The WAVEWATCHIII® Development Group (WW3DG), 2016: User manual and system documentation of WAVEWATCHIII® version 5.16. Tech. Note 329, NOAA/NWS/NCEP/MMAB, College Park, MD, USA, 326 pp.

Implications of different ocean color products in a global ocean model: Sensitivity analyses for NINO3.4 region

Hae-Cheol Kim[1,*], Avichal Mehra[2], Sudhir Nadiga[1], Zulema Garraffo[1], Seunghyun Son[3], Eric Bayler[4]

[1]IMSG at NWS/NCEP/EMC, [2]NWS/NCEP/EMC, [3]CIRA at NESDIS, [4]NESDIS

Email: Hae-Cheol.Kim@noaa.gov; Phone: 301-683-3700

This is a study funded by Joint Polar Satellite System (JPSS) - Proving Ground and Risk Reduction (PGRR) Program at NOAA's National Environmental Satellite, Data, and Information Service (NESDIS). The main motivation of this study is to demonstrate how various ocean color products can be used in a global ocean modeling framework [1], and to investigate effects of different combinations of atmospheric forcings (Climate Forecasting System Reanalysis (CFSR) [2]; Reanalysis 2 (RA2) [3]) and ocean color products on the upper water thermal structure of the NINO3.4 region (5°N - 5°S and 170°W - 120°W).

Two ocean color (OC) products (Sea-Viewing Wide Field-of-View Sensor (SeaWiFS); Visible Infrared Imager Radiometer Suite (VIIRS)) and two different optical algorithms for computed short-wave radiant fluxes [4][5] are used for computing shortwave radiant fluxes in water, and they were combined with two different atmospheric forcings (CFSR and RA2) for creating eleven numerical experiments of a global ocean model (Table 1). Effects of different optical parameterizations and frequencies of ocean color products along with different forcings on the upper ocean thermal structure are then quantitatively compared.

Table 1. Various ocean color products and temporal frequencies used for computing short wave radiant fluxes combined with different atmospheric forcings in a global ocean modeling framework (H: hourly data used; D: daily-averaged data used; SH; simulated hourly data used for shortwave radiant fluxes only; SZA: solar zenith angle).

Experiments	Ocean color product	Sensor	Forcings	OC Period	Algorithms
KparCLM	Long-term climatological K_{dPAR} [6]	SeaWiFS	CFSR (H)	1997-2010	[4]
ChlaCLM	Long-term climatological Chl-a [7]	SeaWiFS	CFSR (H)	1997-2010	[5]
ChlaIND	Interannual mean Chl-a [7]	SeaWiFS	CFSR (H)	Each year (2001 – 2010)	[5] No diurnal SZA in water
ChlaID	Interannual mean Chl-a [7]	SeaWiFS	CFSR (H)	Each year (2001 – 2010)	[5] Diurnal SZA in water
KparSWFclmD	Long-term climatological K_{dPAR} [6]	SeaWiFS	RA2 (D)	1997-2010	[4]
KparVRSclmD	Long-term climatological K_{dPAR} [6]	VIIRS	RA2 (D)	2012-2015	[4]
KparVRSclmH	Long-term climatological K_{dPAR} [6]	VIIRS	RA2 (SH)	2012-2015	[4]
ChlaSWFclmD	Long-term climatological Chl-a [7]	SeaWiFS	RA2 (D)	1997-2010	[5] No diurnal SZA in water
ChlaVRSclmD	Long-term climatological Chl-a [7]	VIIRS	RA2 (D)	2012-2015	[5] No diurnal SZA in water
ChlaVRSclmH	Long-term climatological Chl-a [7]	VIIRS	RA2 (SH)	2012-2015	[5] No diurnal SZA in water
ChlaVRSclmDW	Long-term climatological Chl-a [7]	VIIRS	RA2 (D)	2012-2015	[5] Diurnal SZA in water

Hybrid Coordinate Ocean Model (HYCOM; GLBa0.24 hereafter) with cylindrical (78.64°S – 66°S); recti-linear coordinate (66°S – 47°N); and. Arctic bipolar patch (>47°N) is used. HYCOM has vertical coordinates employing 32 layers with following isopycnals in the deep sea, z-levels in the surface and terrain-following σ-coordinate near coastal areas [1]. K-Profile Parameterization (KPP) [8] is used as a vertical mixing scheme. GLBa0.24 is forced by either hourly atmospheric fluxes from NOAA's CFSR [2] or daily averaged RA2 [3]. Temperature averaged over the upper 100m at the NINO3.4 region is selected to quantify the impact of each numerical runs, and Global Ocean Data Assimilation System (GODAS) [9] is used for verification purposes.

All experiments are divided into two large groups: SeaWiFS-CFSR (red fonts in Table 1) and VIIRS-RA2 combination (blue fonts in Table 2), respectively. The first four numerical experiments in Table 1 (KparCLM; ChlaCLM; ChlaIND; and ChlaID) belong to SeaWiFS-CFSR combination, where, the last seven experiments (KparSWFclmD; KparVRSclmD; KparVRSclmH; ChlaSWFclmD; ChlaVRSclmD; ChlaVRSclmH; and ChlaVRSclmDW) are from the second group. Simulation period for the first group is 2001-2009 and for the second group is 2012-2015, respectively.

In summary, the comparison of the first group against GODAS product reveals that algorithmic differences (KparCLM versus ChlaCLM, ChlaIND, ChlaND) are noticeable, and that KparCLM yields better results with respect to root mean squared difference (RMSD) and correlation (Fig. 1a). Comparisons between the members in the second group and GODAS indicate that neither ocean color products nor algorithms used for shortwave radiation seem to have much impact (Fig. 1b) in improving simulated results or changing the thermal structure. However, it should be noted that temporal frequency of shortwave radiant fluxes (simulated hourly versus daily) makes noticeable differences in the top 100m averaged temperatures of the NINO3.4 region (Fig. 1b).
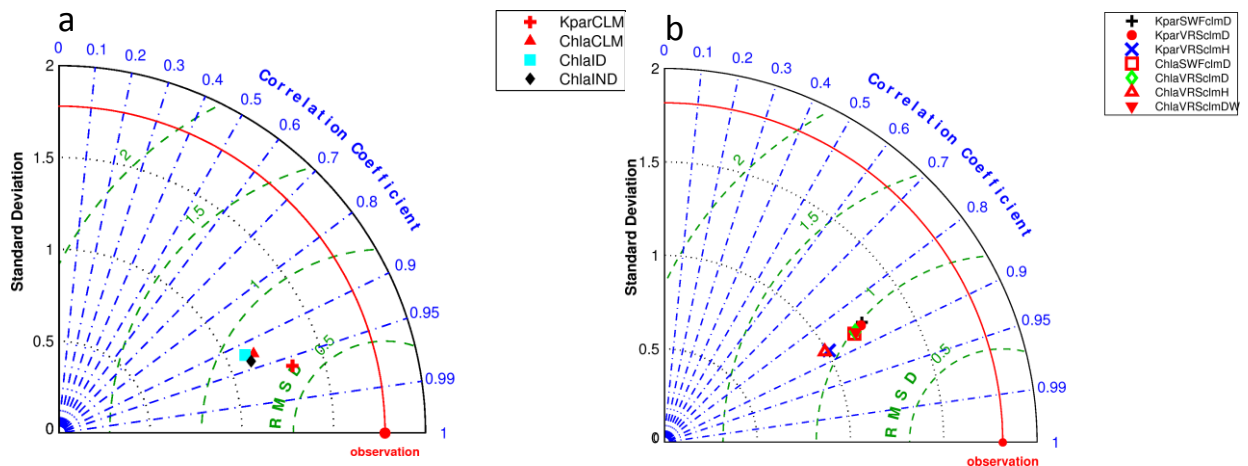
Fig. 1. Taylor diagrams for comparisons of all numerical experiments against GODAS. Comparisons between members of the first group (a) and the second group (b) with GODAS are presented, respectively.

[1] Bleck, R., 2002: An oceanic general circulation model framed in hybrid isopycnic-Cartesian coordinates, Ocean Model., 37, 55-88.
[2] Saha, S., *et al.* (2010) The NCEP climate forecast system reanalysis. Bull. Amer. Meteor. Soc., 91, 1015–1057.
[3] Kanamitsu, M., W. Ebisuzaki, J. Woollen, S Yang, J. Hnilo, M. Fiorno, and G. Potter (2002) NCEP-DOE. AMIP-II Reanalysis (R-2). Bull. Amer. Meteor. Soc., 83, 1631-1643.
[4] Kara, A.B., H.E. Hurlburt, P.A. Rochford, and J.J. O'Brien (2004). The impact of water turbidity of the interannual sea surface temperature simulations in a layered global ocean model. J. Phys. Oceanogr., 34, 345–359.
[5] Lee, J., K. Du, R. Arnone, S. Liew, and B. Penta (2005), Penetration of solar radiation in the upper ocean: A numerical model for oceanic and coastal waters, J. Geophys. Res., 110, 1-12.
[6] Son, S. and M. Wang (2015) Diffuse attenuation coefficient of the photosynthetically available radiation Kd(PAR) for global open ocean and coastal waters, Remote Sens. of Environ., 159, 250-258.
[7] O'Reilly, J.E., S. Maritorena, B.G. Mitchell, D.A. Siegel, K L. Carder, S. A. Garver, M. Kahru, and C. McClain (1998), Ocean color chlorophyll algorithms for SeaWiFS, J. Geophys. Res., 103, 24,937-24,954.
[8] Large, W.C., J.C. McWilliams and S.C. Doney, 1994: Oceanic vertical ixing: a review and a model wit a nonlocal boundary layer parameterization. Rev. Geophys. 32, 363-403.
[9] Behringer, D. W., and Y. Xue (2004) Evaluation of the global ocean data assimilation system at NCEP: The Pacific Ocean. Eighth Symposium on Integrated Observing and Assimilation Systems for Atmosphere, Oceans, and Land Surface, AMS 84th Annual Meeting, Washington State Convention and Trade Center, Seattle, Washington, 11-15.

Using Neural Networks for Nonlinear Averaging NCEP Wave Model Ensemble

V. Krasnopolsky[1], R. Campos[2], J.H. Alves[3], S. Penny[2]

[1]NWS/NCEP/EMC, [2]AOSC/UMD, [3]NCEP/EMC/SRG

Email: vladimir.krasnopolsky@noaa.gov; Phone: 301-683-3742

The NCEP Global Wave Ensemble System (GWES) was implemented in 2005 [1] and initially validated by [2]. After upgrades reported in [3], it is now run with four cycles per day, using a spatial grid with 0.5° resolution, with forecast range to 10 days. A total of 20 perturbed members plus a control member compose the GWES, which consists of an implementation of the WAVEWATCH III model [4], forced by winds from NCEP's Global Ensemble Forecast System (GEFS) [5]. A recent assessment and comparison of deterministic and ensemble products using altimeter data is provided in [3]. Their results show that although the general bias of the ensemble system does not show significant improvement over the deterministic global wave, after the fifth forecast day, root mean square errors from the GWES become smaller than the deterministic run. Furthermore, the GWES continuous ranked probability scores (CRPS) systematically outperforms the corresponding deterministic model's mean absolute error (MAE) in all forecast times.

In the current study, we propose an improvement of the quality of output products from the GWES using neural networks (NN), which are initially used to compute nonlinear averages. Currently a conservative ensemble approach is used to calculate the ensemble mean (EM) in the GWES. The ensemble mean for variable p is calculated as,

$$EM = \frac{1}{n}\sum_{i=1}^{n} p_i \tag{1}$$

here n is the number of ensemble members and p_i is the i-th ensemble member.

An improvement upon (1) can be achieved using weighted EM (WEM),

$$WEM = \frac{\sum_{i=1}^{n} W_i \cdot p_i}{\sum_{i=1}^{n} W_i} \tag{2}$$

where W_i are weights subscribed to ensemble members. A priori information can be used to select the weights W_i. In addition, if observational data are available for the variable p, eq. (2) can be considered as a linear regression. Solving the linear regression equations (2), W_i and the linear regression EM (LREM) can be found. Eq. (2) assumes a linear relationship between EM and the ensemble members; however, in reality, this relationship may be significantly nonlinear, and we can use a nonlinear statistical tool like NN to derive a relationship between ensemble members and nonlinear EM (NEM),

$$NEM = NN(p_1, p_2, \cdots, p_n) \tag{3}$$

In a previous work [6], we demonstrated that a NN technique can be successfully used for averaging multi-model ensemble for precipitation over the Continental US. We showed that NN provides significantly better results than conservative ensemble or LREM. In fact, NN results are comparable with those obtained by a human meteorologist-analyst. In this pilot study, we apply NN to calculate NEM in GWES.

To start with, we selected a "one buoy location" setup. We used 21 GWES ensemble members from a single grid point near the buoy location at 32.501N and 79.099W (buoy #41004 in the North Atlantic Ocean, water depth of 37 meters); distant only 9.7 km to the nearest model grid point selected. As inputs to our NN we use three model variables related to 5-day forecasts for: significant wave height, H_s, peak period T_p, and wind speed at 10 m height, U_{10}, a total of 63 (3 x 21) inputs. Also, two metavariables: sin and cos of the day of the year were used. Thus, our NN has 65 inputs in total. The NN has three outputs: H_s, T_p, and U_{10}. One year of data for buoy #41004 was used for training the NN outputs. For NN validation we used one year of data collected at buoy #41013, located at a distance of about 100 mi from buoy #41004.

Table 1. Performance of three ensembles (1) to (3) for H_s on independent validation set (buoy #41013). MAE is mean absolute error, SI – scatter index, CC – correlation coefficient, and Max the largest value of H_s in m.

	Bias	RMSE	MAE	SI	CC	Max
Conservative EM	-0.03	0.445	0.301	0.334	0.759	6.28
LREM	0.28	0.463	0.313	0.348	0.754	4.46
NEM	0.12	0.424	0.29	0.328	0.782	4.3
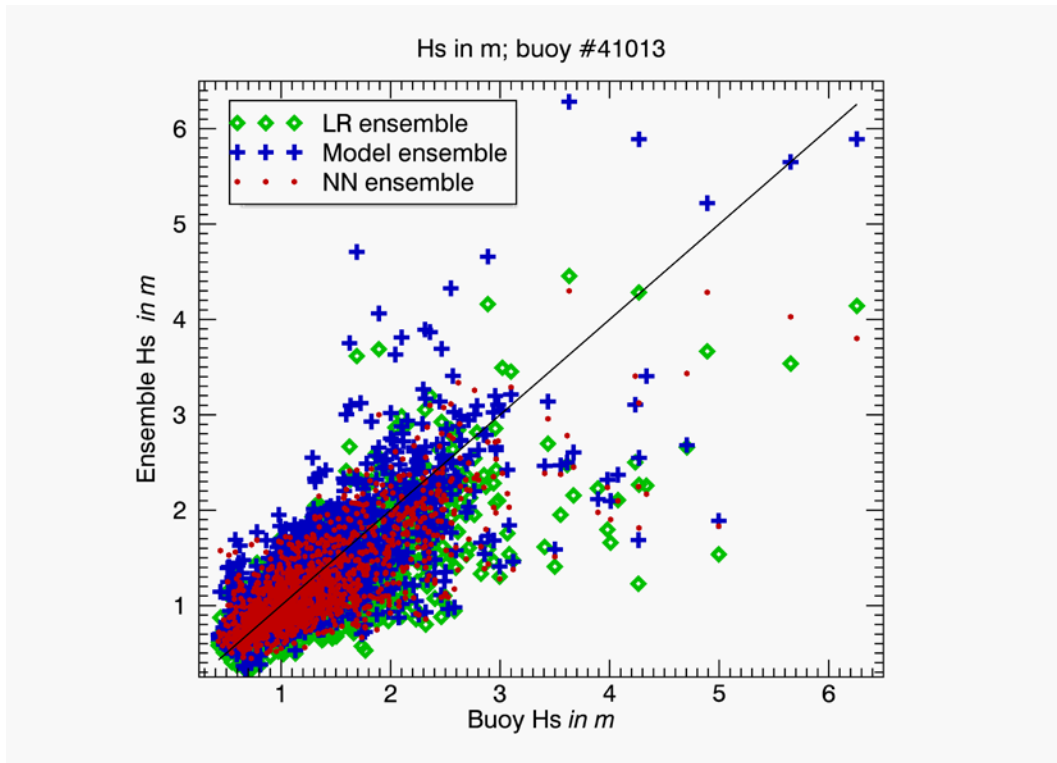
Figure 1 - Scatter plot shows three overlaid scatterplots: blue crosses show wave model ensemble, green diamonds – LREM, and red dots – NEM.

Table 1 shows comparison of three aforementioned ensembles relative to an independent validation set (buoy #41013). NEM outperforms the model ensemble and LR ensemble for all statistics except the max value. Fig. 1 illustrates the reason: there are very few data points with $H_s > 3$ m. These data are not sufficient for NN (and LR) training in the area of high H_s.

As the next step, our investigation will move from one buoy configuration to two regional (Atlantic and Pacific) configurations and, eventually, to a global configuration when one or several NNs will provide NEM over the entire global ocean. In addition, we are going to include the altimeter data in the training process.

References

[1] Chen, H. S., 2006: Ensemble prediction of ocean waves at NCEP. Proc. 28th Ocean Engineering Conf., Taipei, Taiwan, NSYSU, 25–37.

[2] Cao, D., H. S. Chen, and H. L. Tolman, 2007: Verification of ocean wave ensemble forecasts at NCEP. Proc. 10th Int. Workshop on Wave Hindcasting and Forecasting and First Coastal Hazards Symp., Oahu, Hawaii, G1.

[3] Alves, J.H.G.M., Wittman, P., Sestak, M., Schauer,J., Stripling, S., Bernier, N.B., McLean, J., Chao, Y., Chawla, A., Tolman, H., Nelson, G., Klots, S., 2013. The NCEP–FNMOC combined wave ensemble product. Expanding Benefits of Interagency Probabilistic Forecasts to the Oceanic Environment. Bull. American Met. Society, BAMS, December 2013.

[4] WAVEWATCH III® Development Group, 2016: User manual and system documentation of WAVEWATCH III® version 5.16. Tech. Note 329, NOAA/NWS/NCEP/MMAB, College Park, MD, USA, 326 pp. + Appendices.

[5] Hou, D., Z. Toth, Y. Zhu, and Y. Yang, 2008: Impact of a Stochastic Perturbation Scheme on NCEP Global Ensemble Forecast System. Proceedings, 19th AMS conference on Probability and Statistics. New Orleans, LA, 20-24 Jan. 2008.

[6] Krasnopolsky V., and Y. Lin, 2012: "A Neural Network Nonlinear Multimodel Ensemble to Improve Precipitation Forecasts over Continental US", Advances in Meteorology, Volume 2012, Article ID 649450, 11 pages, doi:10.1155/2012/649450

Oceanic internal waves internally generated in a 0.1° OGCM

Thomas Reitz[1], Jin-Song von Storch[1]
[1]Max Planck Institute for Meteorology, Hamburg, Germany
Email: thomas.reitz@mpimet.mpg.de

Introduction

The ocean is full of mesoscale eddies continuously generated by barotropic and baroclinic instabilities. How the eddying flows dissipate their energy is not well understood. Since mesoscale eddies tend to transfer their energy towards larger scales (Charney, 1971), processes other than quasi-geostrophic turbulence are necessary to dissipate the energy of eddying flows in an equilibrium state. Müller et al. (2005) referred to this as the ocean's route to dissipation. One way to dissipate the energy of eddying flows is to generate internal gravity waves. These internally generated waves can transfer the energy towards smaller scales via non-linear wave-wave interactions or wave breaking. Internally generated internal waves can emerge from unbalanced flows (Molemaker et al., 2010), interactions with bottom topography (Nikurashin et al., 2013) or from spontaneous imbalance. This work investigates such an energy pathway using simulations with the 0.1° Max Planck Institute Ocean Model (MPIOM). Note that externally generated internal waves, such as wind-induced near-inertial waves or internal tides, are not directly linked to eddying flows and hence may not directly participate in the dissipation of the energy of these flows.

Two simulations have been performed with the MPIOM, using a tripolar grid with a horizontal resolution of 0.1°. The simulations start from an existing multi-decadal NCEP-forced simulation (von Storch et al. 2012), in which the eddying flows are fully developed. They cover a time period of three months in 2005: June, July and August. In the first simulation (exp_6h) the ocean is driven by the fluxes derived from 6 hourly NCEP data. In the second simulation (exp_const) the ocean is driven by constant fluxes obtained by averaging the same fluxes over the three months. In both simulations, the tides are switched off. Thus, exp_const excludes all external forcing factors which otherwise would lead to externally generated internal waves. The results shown in the following are all taken from the August data.

Results

Figure 1 shows the fraction of energy in the eddying flows relative to the total kinetic energy on the left and the fraction of internal wave energy relative to the total kinetic energy on the right for exp_6h at 100 m. In figure 2 the fraction of exp_const relative to exp_6h is shown for the eddy energy on the left and the internal wave energy on the right, both also at 100 m. Energy of eddying flows/internal wave energy is defined as the variance of meridional and zonal velocity fluctuations on time scales longer/shorter than the local inertial period. On the one hand both experiments have a comparable amount of energy in the eddying flows. The ratio of eddy kinetic energy in exp_const to the one in exp_6h is around one (Fig. 2, left) in regions with strong eddy kinetic energy (Fig. 1, left). Thus the constant surface forcing does not kill the eddies. On the other hand the internal wave energy in exp_6h is much higher than in exp_const. In exp-6h, internal wave energy is strong (Fig. 1, right) in the tropical and subtropical regions outside strong currents with high eddy activities in the Gulf Stream, the Kuroshio and the Antarctic Circumpolar Current. This is consistent with the idea that the wind-induced near-inertial waves, once being generated in the storm track regions, propagate equatorward and enhance super-intertial variability there. Under constant surface forcing, the wind-induced near-inertial waves are strongly reduced.

Nevertheless, notable internal wave energy is found in tropical regions and in regions where high eddy activity is present (Fig. 2, right). In both cases the internal wave energy in exp_const is comparable to the one in exp_6h. In regions of high eddy activity the internal waves are likely spontaneously emitted by the eddying flows and then captured by the flows. The generation of the internal waves in the equatorial regions may be different from the one in high-eddy-activity regions, because there the energy of eddies is much smaller than the energy of the internal waves. Additionally the Rossby numbers in tropical regions are not as small as in the extratropical regions, thus the flow is probably not as well balanced in this region. Further research is needed to investigate the source of internal waves occurring there.
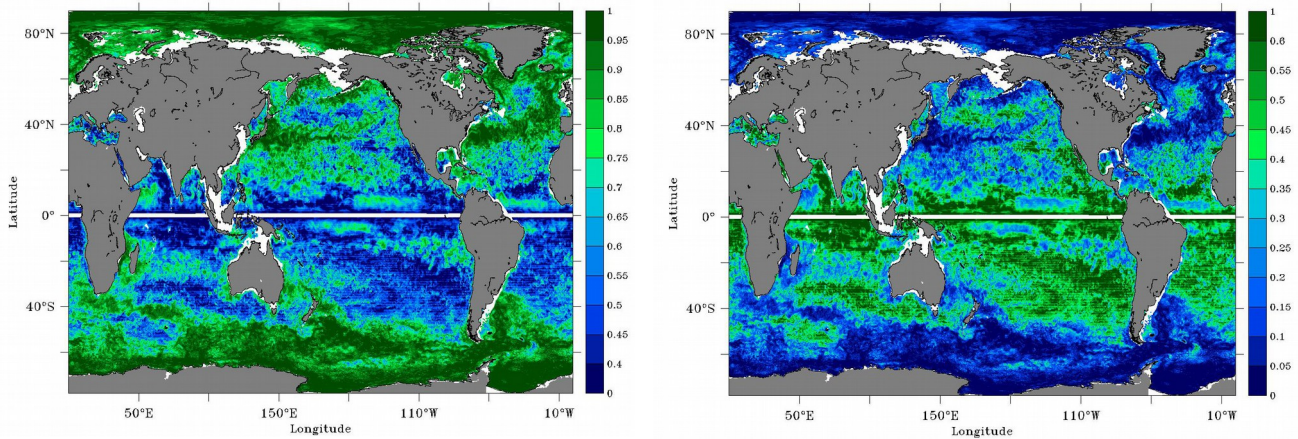
Figure 1: Fraction of energy relative to the total kinetic energy for exp_6h (left: eddy, right: internal wave)
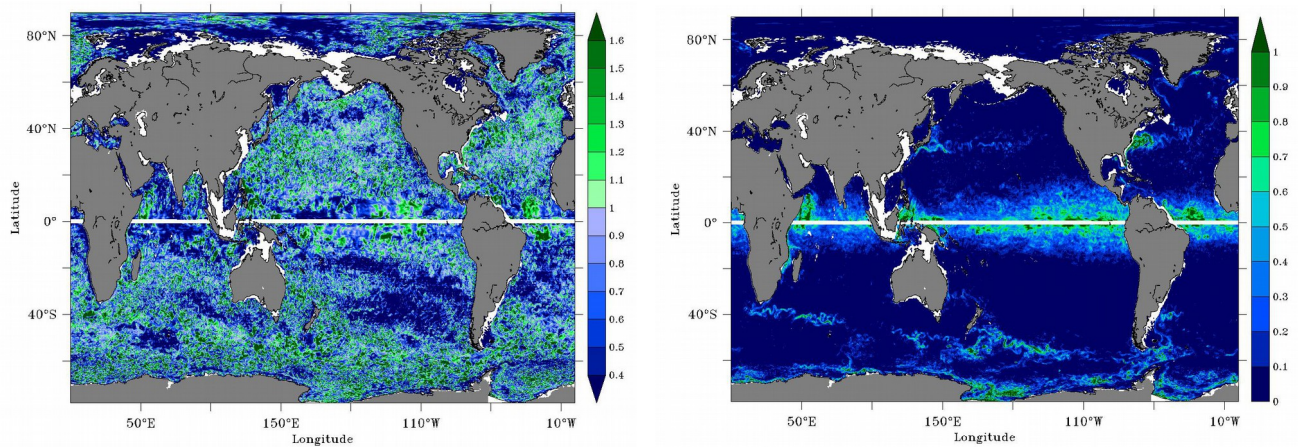
Figure 2: Fraction of energies in exp_const relative to the energies in exp_6h (left: energy of eddying flows, right: internal wave energy)

References

Charney, J. G. (1971). Geostrophic turbulence. J. Atmos. Sci., 28(6):1087–1095.

Molemaker, M. J., McWilliams, J. C., and Capet, X. (2010). Balanced and unbalanced routes to dissipation in an equilibrated Eady flow. Journal of Fluid Mechanics, 654:35–63.

Müller, P., McWilliams, J. C., and Molemaker, M. J. (2005). Routes to dissipation in the ocean: The 2D/3D turbulence conundrum. In Baumert, H. Z., Simpson, J., and Sündermann, J., editors, Marine Turbulence, pages 397–405. Cambridge University Press.

Nikurashin, M., Vallis, G. K., and Adcroft, A. (2013). Routes to energy dissipation for geostrophic flows in the Southern ocean. Nature Geoscience, 6:48–51.

von Storch, J.-S., Eden, C., Fast, I., Haak, H., Herńandez-Deckers, D., Maier-Reimer, E., Marotzke, J., and Stammer, D. (2012). An Estimate of the Lorenz Energy Cycle for the World Ocean Based on the STORM/NCEP Simulation. Journal of Physical Oceanography, 42:2185–2205.